Vol. 92 No. 2 pp. 769–785 ACTA GEOLOGICA SINICA (English Edition) Apr. 2018

Tectonically-controlled Evolution of the Late Cenozoic Nihewan Basin, North China Craton: Constraints from Stratigraphy, Mineralogy, and Geochemistry

LIU Jin[1, 2], CHEN Xingqiang[3, 4, *], CHI Zhenqing[2], WANG Yong[2], MIN Longrui[2] and LI Tingdong[2]

1 *School of Civil and Architecture Engineering, Xi'an Technological University, Xi'an 710021, China*
2 *Institute of Geology, Chinese Academy of Geological Sciences, Beijing 100037, China*
3 *China Railway First Survey and Design Institute Group CO., Ltd., Xi'an 710043, China*
4 *Institute of Geomechanics, Chinese Academy of Geological Sciences, Beijing 100081, China*

Abstract: The Late Cenozoic basins in the Weihe–Shanxi Graben, North China Craton are delineated by northeast-striking faults. The faults have, since a long time, been related to the progressive uplift and northeastward expansion of the Tibetan Plateau. To show the relation between the basins and faults, two Pliocene–Pleistocene stratigraphic sections (Chengqiang and Hongyanangou) in the southern part of the Nihewan Basin at the northernmost parts of the graben are studied herein. Based on the sedimentary sequences and facies, the sections are divided into three evolutionary stages, such as alluvial fan-eolian red clay, fan delta, and fluvial, with boundaries at ~2.8 and ~1.8 Ma. Paleocurrent indicators, the composition of coarse clastics, heavy minerals, and the geochemistry of moderate–fine clastics are used to establish the temporal and spatial variations in the source areas. Based on features from the middle-northern basin, we infer that the Nihewan Basin comprises an old NE–SW elongate geotectogene and a young NW–SE elongate subgeotectogene. The main geotectogene in the mid-north is a half-graben bounded by northeast-striking and northwest-dipping normal faults (e.g., Liulengshan Fault). This group of faults was mainly affected by the Pliocene (before ~2.8–2.6 Ma) NW–SE extension and controlled the deposition of sediments. In contrast, the subgeotectogene in the south was affected by northwest-striking normal faults (e.g., Huliuhe Fault) that were controlled by the subsequent weak NE–SW extension in the Pleistocene. The remarkable change in the sedimentary facies and provenance since ~1.8 Ma is possibly a signal of either weak or strong NE–SW extension. This result implies that the main tectonic transition ages of ~2.8–2.6 Ma and ~1.8 Ma in the Weihe–Shanxi Graben are affected by the Tibetan Plateau in Pliocene–Pleistocene.

Key words: sedimentation, extension, Neotectonic, Weihe-Shanxi Graben, Tibetan Plateau

1 Introduction

The Weihe–Shanxi Graben in the southeastern Ordos Block, North China Craton (Fig. 1a) is one of the most significant seismic zones of eastern Asia (Deng and You, 1985; Xu et al., 1993; Zhang et al., 1999; Zhang et al., 2003). The neotectonic evolution has, since a long time, been related to the evolution of the Tibetan Plateau (Peltzer et al., 1985; Tapponnier et al., 1986; Zhang et al., 1998; Zhang et al., 2003; Sun, 2005; Yin, 2010; Chen et al., 2015, 2016). In contrast to the strong deformation of the strata in the western margin of the Ordos Block (Wang et al., 2013; Li et al., 2015; Shi et al., 2015a), only brittle fracturing recorded in the graben owing to the Tibetan Plateau (Zhang et al., 2003; Cen et al., 2015; Shi et al., 2015b; Chen et al., 2015, 2016). The exact timing of the regional stress transition remains poorly understood because of the hard dating for brittle fracturing. This uncertainty has prevented us from understanding the relation between the basin evolution and regional stresses owing to the Tibetan Plateau. Because the graben currently fills with sediments from the neighboring mountains, it is natural to use the Cenozoic strata to decipher the role of the basin-controlling faults and the uplift history of the mountains.

The Nihewan Basin (Figs. 1b and 1c), situated in the

* Corresponding author. E-mail: cxq123111@163.com

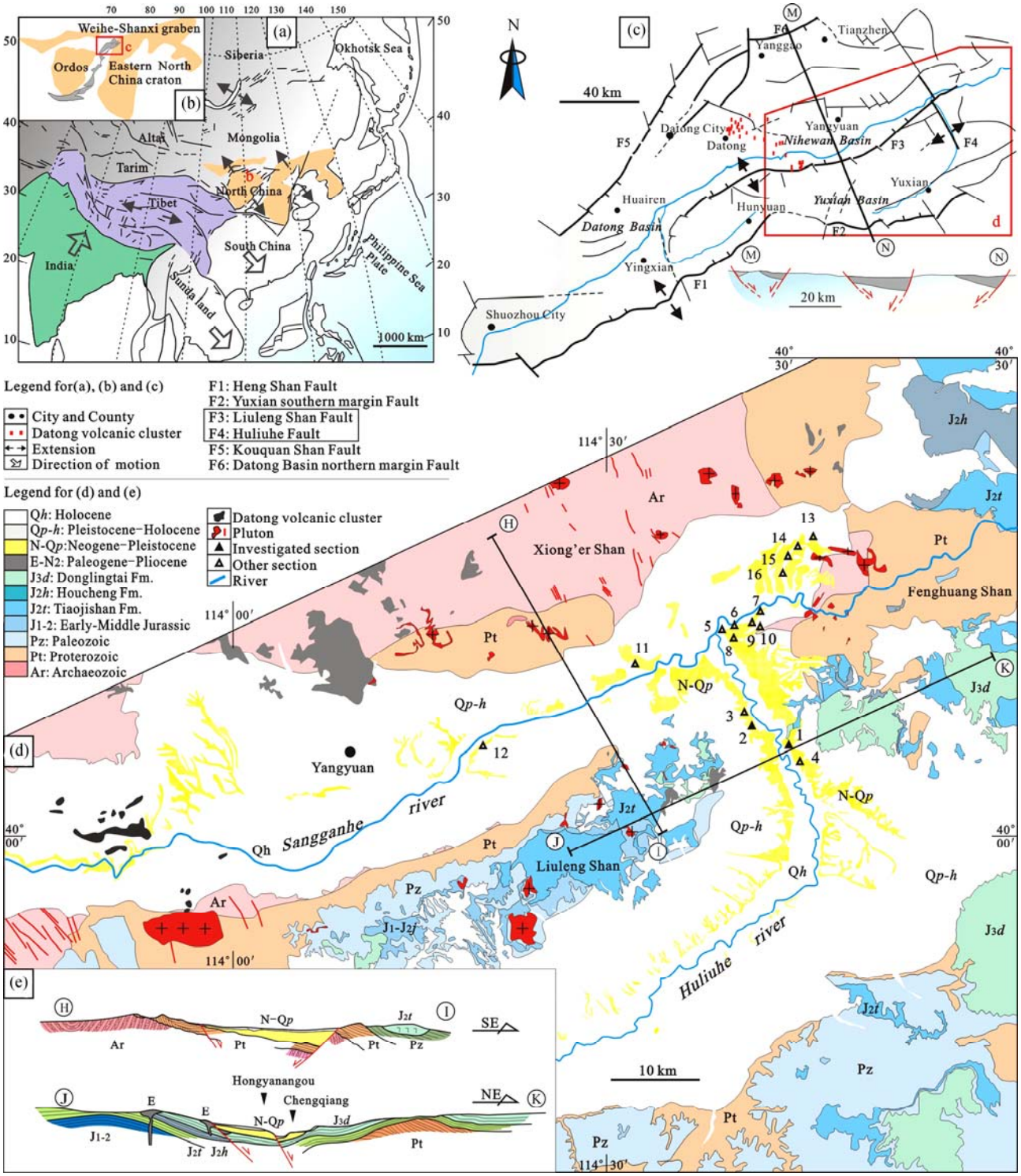

Fig. 1. (a), Active tectonics and neotectonics of Asia (modified from Tapponnier et al. (1986) and Zhang et al. (2003)). (b), Location of the Weihe-Shanxi Graben in North China. (c), Simplified structural map of the Datong-Yangyuan Basin showing the structural framework of the Nihewan Basin (after Wang et al. (1996) and Zhang et al. (1998)). (d), Simplified geologic map of the Nihewan Basin showing the locations of the studied sections. (e), Cross sections showing the middle-northern part of the Nihewan Basin as a maingeotectogene (H-I) and the southern part as a subgeotectogene (J-K).

Sections: 1, Chengqiang; 2, Hongyanangou; 3, Daodi; 4, Dongyaozitou; 5, Xiaodukou; 6, Haojiatai (HJT); 7, Donggutuo; 8, Taiergou (TEG1) and Eastern Taiergou (TEG2); 9, Xiaochangliang; 10, Majuangou; 11, Hutouliang; 12, Jin'erwa; 13, Northeastern Shangshagou (SSG2); 14, Southwestern Shangshagou (SSG1); 15, Southwestern Wulitai (WLT); 16, Xiashagou (XSG).

northernmost of the Weihe–Shanxi Graben, is the most important Pliocene–Quaternary location for mammalian fossils in North China (Huang and Tang, 1974; Du et al., 1988; Cai et al., 2007). Magnetostratigraphy (Su et al., 2000; Zhu et al., 2004; Min et al., 2006; Wang et al., 2006; Chi et al., 2010) and paleontology (Wang, 1982; Du et al., 1988, 1995) has been used to constrain the strata deposition. Previous studies on sedimentation have focused on the mid-northern basin, including the sections of Eastern Taiergou, Xiashagou, Southwestern Wulitai, Southwestern Shangshagou, Northeastern Shangshagou, and Hutouliang (Fig. 1d) (Wang, 1989; Chen et al., 2012, 2015; Han et al., 2016). Based on these sections, a three-stage basin evolution model in Pliocene–Pleistocene was proposed (Chen et al., 2015). To constrain the evolution of the southern basin, the sediments, heavy minerals, and geochemistry of two middle Pliocene–Pleistocene sections (Chengqiang and Hongyanangou) (Figs. 1d and 1e) are studied, and a self-consistent model for the temporal and spatial evolution of the basin is presented. Finally, the main transition ages owing to the tectonics of the Tibetan Plateau in the Weihe–Shanxi Graben are proposed.

2 Geological Setting

The Nihewan Basin is an NE–SW elongate geotectogene bounded by the normal NE-striking Liulengshan Fault to the south (Chen, 1987; Wang et al., 1996; Shi et al., 2015b). The basin is connected to the Datong Basin in the southwest and the Yuxian Basin in the south by the Sangganhe River and Huliuhe River, respectively. The Xiong'er and Liuleng–Fenghuang Mountains are situated at the northwest and southeast of the basin, respectively (Fig. 1d).

Based on the geological map (Figs. 1d and 1e), Archean (Ar) metamorphic rocks and Proterozoic (Pt) sedimentary rocks are preserved in the Xiong'er Mountains. Proterozoic (Pt) and Early Paleozoic (Pz) sedimentary rocks are exposed in the northwest of the Liuleng Mountains, whereas Lower–Middle Jurassic sedimentary rocks (J_{1-2}), andesite (J_2t), Paleogene dolerite, and basalts are exposed in the southeast of the Liuleng Mountains. In Fenghuang Shan, Proterozoic sedimentary rocks are exposed in the north, Middle Jurassic andesite (J_2t) in the middle, and Middle–Upper Jurassic rhyolite (J_3d) and tuff (J_2h) in the south. The Neogene–Pleistocene (N-Q*p*) fluvial–lacustrine "Nihewan beds" are exposed along the Sangganhe and Huliuhe Rivers and are overlain by Pleistocene–Holocene eolian, alluvial, and fluvial sediments.

3 Stratigraphy and Ages of the Studied Sections

The 96-m thick Chengqiang section mainly comprises yellow sands and gray conglomerates, with a small amount of mud and silt. Mammalian fossils assemblages such as *Hypolagus cf. H. schreuderi, Nannocricetus mongolicus, Sinocricetus progressus, Micromys sp., Mesosoiphneus sp., Pliosiphneus sp., and Pseudomeriones complicidens* in Pliocene (Du et al., 1988; Cai et al., 2007) and *O. cf. O. youngi*, *Allophaiomys cf., A. pliocuenicus, and Yangia sp.* in Early Pleistocene (Cai et al., 2007) have been found. Magnetostratigraphic data suggest that sediments of this section were deposited from ~3.1 Ma ago (Li and Wang, 1982) (Figs. 2 and 3).

The 119-m thick Hongyanangou section and the Chengqiang section share the same lithology. The main Pliocene mammalian fossils are the *Proboscidipparion sinensis (Hipparion sp.)* and *Chilotherium sp.* (Huang and Tang, 1974). In addition, some trace fossils (burrows) and ostracodes (Chen, 1988) have been found in some layers. Magnetostratigraphic data suggest that these sediments were deposited from ~3.6 Ma ago (Cheng et al., 1978; Chen, 1988) (Figs. 2 and 3). Deng et al. (2008) proposed a younger depositional age (~2.8 Ma) for the adjacent Hongya section than the Hongyanangou section. Based on the lithology and sedimentary structures, except for the

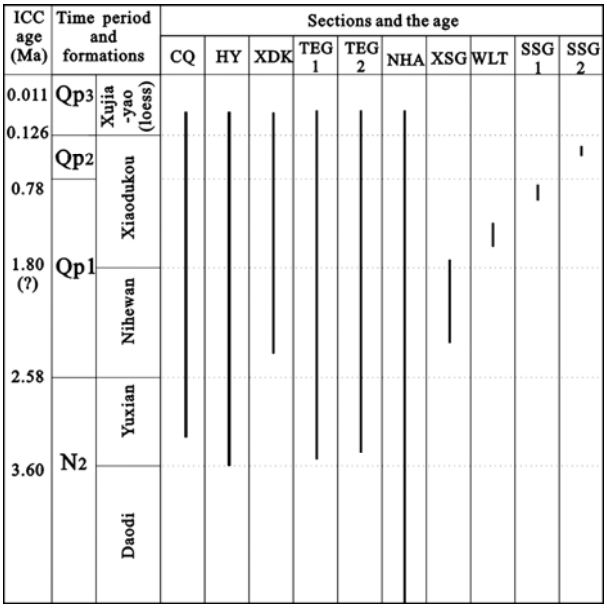

Fig. 2. Stratigraphic framework of the studied sections in the Nihewan Basin.

Formations followed Chen et al. (2015). Ages of section: CQ is from Li and Wang (1982) and Du et al. (1995), HY is from Chen (1988) , TEG1 is from Min et al. (2006), TEG2 is from Chen et al. (2012), and XSG, WLT, SSG1 and SSG2 are from Chen et al. (2015). For detailed information of the magnetostratigraphic ages of Chengqiang and Hongyanangou sections, see Fig. 3.

upmost 2–3-m thick loess, both sections can be divided into three units with boundaries ages at ~2.8 (lower) and ~1.8 Ma (upper).

4 Sampling and Analytical Methods

4.1 Sedimentary environments

Data concerning the lithology, sedimentary structures (mainly beddings and imbricate clasts), colors, and correlations from the Chengqiang and Hongyanangou sections were collected to recognize the sedimentary environment in these sections. In addition, we relied on literature data from five sections and one core (Chen et al., 2012, 2015; Min et al., 2015).

4.2 Paleocurrent indicators and conglomerates components

Cross-bedding and imbricate clasts are direct paleocurrent indicators in fluvio–lacustrine sediments. Data for cross-bedding were collected from five locations and those for imbricate clasts were collected from three locations in the Chengqiang section. In the Hongyanangou section, cross-bedding data were collected from 12 locations. The lithology of six conglomerate layers in the Chengqiang section and seven conglomerate layers in the Hongyanangou section were analyzed to identify the source rocks. The clasts were classified into four groups. Basalt, andesite, and dolerite were grouped into intermediate–basic magmatic rocks; rhyolite and tuff into intermediate–acidic rocks; limestone and sandstone into sedimentary rocks; and gneiss and schists into metamorphic rocks.

4.3 Detrital heavy minerals

Detrital heavy minerals were collected from two Pliocene medium- to fine-grained sandstone samples,

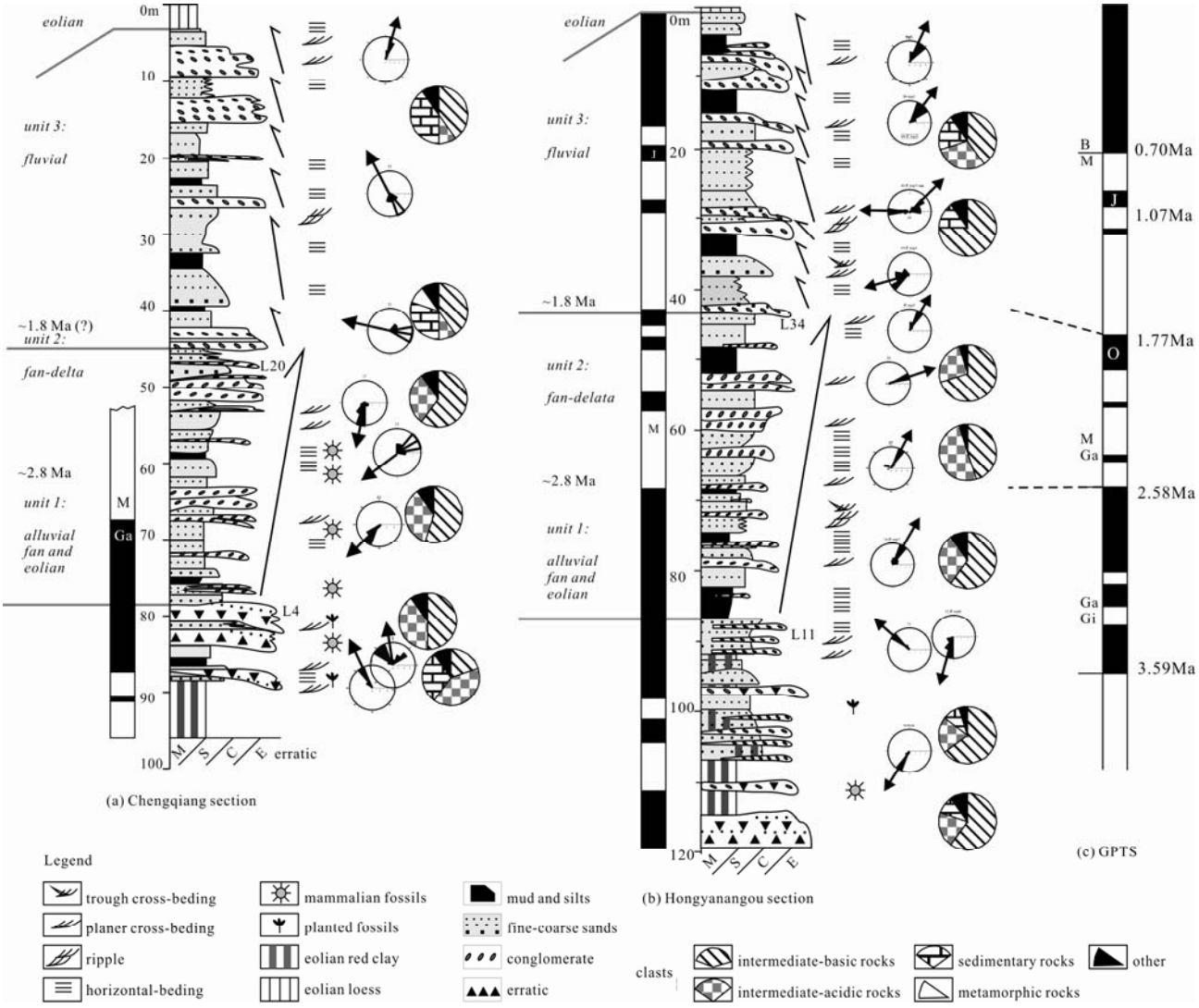

Fig. 3. Sedimentary facies, paleocurrent and clast components of the Chengqiang (a) and Hongyanangou (b) sections.
The GPTS (c) is from Cande and Dennis (1995) and Singer et al. (1999).

three Early Pleistocene fine-grained sandstone samples, and four medium- to fine-grained sandstone samples from the Middle Pleistocene of the Chengqiang section (Fig. 3) for analysis. Twenty-seven and twenty-two samples from the Hongyanangou and Xiaodukou sections (Chen, 1988) were included in the data base. For the separation and preparation of the heavy minerals, we followed the standard procedures described by Morton (Morton, 1985). The samples were first crushed to <2mm fragments in a jaw crusher. To ensure that the separated heavy minerals represent deposited grains and not lithoclasts, we separated the 0.20–0.45-mm fractions via gravitation settling and by applying an electromagnetic field. Heavy minerals were identified and separated under a binocular microscope. The heavy mineral fractions were weighted in a microbalance, and the mass percentages were converted into volume percentages using the average mineral densities.

4.4 Chemistry of the mud and silts

Geochemical sampling of the Chengqiang section was biased toward the fine-grained clastic rocks because they better reflect the source area than the coarse-grained sediments (McLennan, 1989; Yan et al., 2002; Li et al., 2009; Sun et al., 2015, 2016; Li et al., 2016; Yang et al., 2017; Yu et al., 2017; Zhao et al., 2017). Nine silt and three mud samples were collected for whole-rock geochemical analysis. Care was taken to avoid the samples from being affected by weathering, hydrothermal alteration, and mineralization. The samples were crushed into small pieces and then powdered in an agate mill. Major and trace elements, including rare earth elements (REE), were analyzed via standard X-ray fluorescence and inductively coupled plasma mass spectrometry (ICP-MS) in the Analytical Laboratory, Beijing Research Institute of Uranium Geology. Analytical precision and accuracy for major elements are within 1% and those for trace and REE are better than 10%.

5 Results

5.1 Sedimentary sequences and environments of both sections

5.1.1 Unit 1 (~3.6–2.8 Ma)

Unit 1 comprises red silts to fine sands and erratic gray layers (Fig. 4a). Unit 1 is at 96–78 and 119–87-m depth in the Chengqiang and Hongyanangou sections, respectively. The red silts to fine sands are thick and massive, with occasional cross-bedding in a few layers. We interpret them as eolian deposits related to the Pliocene Jingle Formation (red clay) that is exposed in the intermontane basin in the Ordos Block (Xu et al., 2012). The erratic layers are mainly composed of coarse-grained clasts (10–30 cm, max = 100 cm), mixed with sands and silts. The pebbles are clast-supported, poorly sorted, and have either angular or subangular to rounded structure; these pebbles can be interpreted as debris flow. However, thin silt veins with cross-bedding are also found in the conglomerate, which are probably transported by intermittent flows. Thus, Unit 1 is inferred to represent sedimentary deposits in a small depression on the edge of the basin.

5.1.2 Unit 2 (~2.8–1.8 Ma)

Unit 2 comprises yellow silt or green mud in the bottom (Fig. 4b), yellow sands and fine conglomerate in the middle (Fig. 4c), and fine- to coarse-grained conglomerate at the top. This unit is at 78–45 and 87–43-m depth in the Chengqiang and the Hongyanangou sections, respectively. Cross-bedding (Fig. 4c), trough cross-bedding, and horizontal bedding (Fig. 4c) are common in the sand and silt layers. The clasts in the conglomerate layers are poorly sorted, have subangular to angular structure, with clast diameters of approximately 2–5 cm or larger. Imbricate clasts are seen in the conglomerate. Abundant mammalian fossils have been found in this unit. The oxidized nature, low maturity, and hydraulic characteristics of the sediments suggest it deposited in a fan delta.

5.1.3 Unit 3 (after ~1.8 Ma)

Unit 3 comprises multiple cycles of fine-grained brown conglomerates at the bottom, yellowish sands in the middle, and mud and silts at the top (Fig. 4d). Planar cross-bedding, trough cross-bedding, and parallel bedding are common in such structures. In addition, some mammalian fossils have been found in this unit (Du et al., 1988; Cai et al., 2007). The oxidized nature and hydraulic characteristics suggest fluvial deposits (Allen, 1970; Cant and Walker, 1976).

5.2 Paleocurrent and clast components

Paleocurrent changes occurred in both the Chengqiang and Hongyanangou sections (Fig. 3). In the Chengqiang section, the paleocurrent direction was mainly toward the north and northwest in units 1 and 3 and toward the southwest in unit 2. In the Hongyanangou section, the paleocurrent directions changed from the southwest–northwest in unit 1, to the northeast in unit 2, and to the west and north in unit 3.

Lithological facies analysis suggests that the clast components in both sections are predominantly intermediate–basic (basalt, andesite, and dolerite) and intermediate–acidic magmatic rocks (tuff and rhyolite), with a few sedimentary (limestone and sandstone) and metamorphic rocks (Fig. 3). The mainly angular to

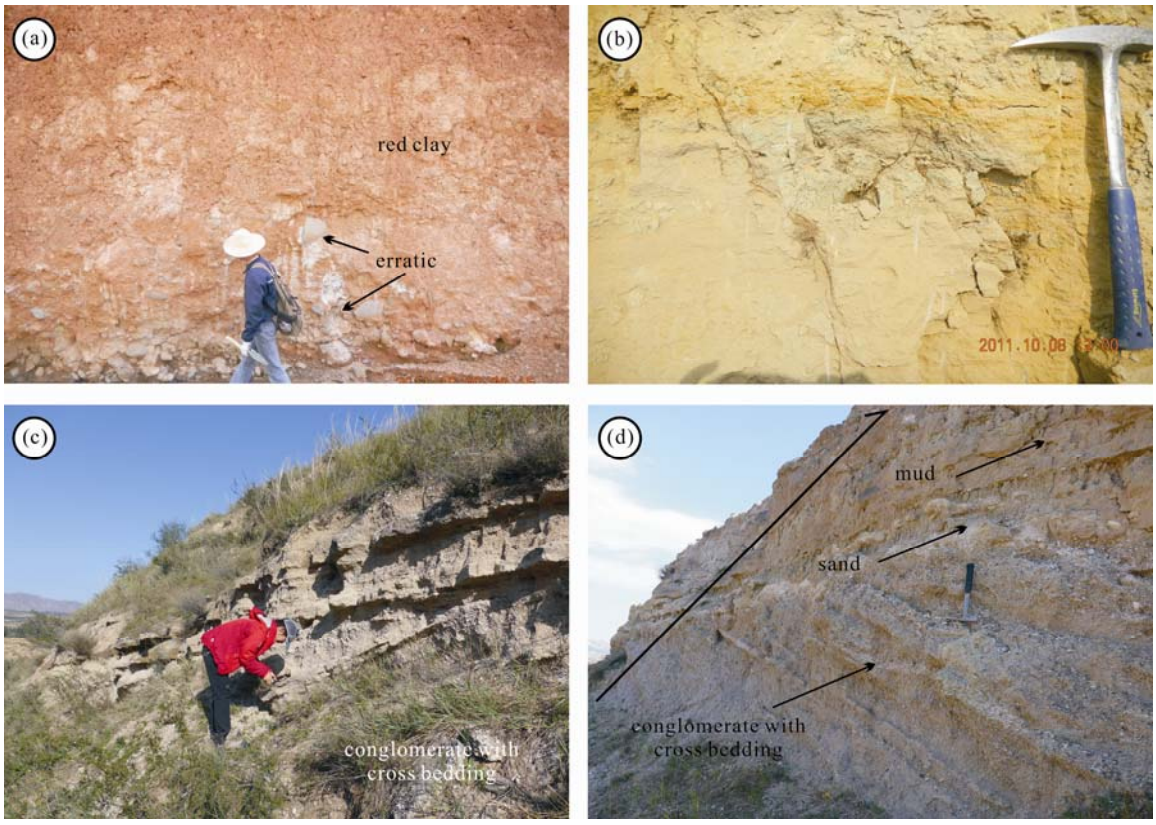

Fig. 4. Field photographs of Chengqiang and Hongyanangou sections showing different sedimentary environments.
(a), Eolian red clay and the erratic in unit 1 of Hongyanangou section. The person is about 1.7 m high in scale. (b), Yellow silts and green mud on the bottom of the fan delta of Chengqiang section. The hammer is about 35 cm long in scale. (c), Planar cross-bedded and horizontal bedded sands in the middle of unit 2 of Hongyanangou section (fan-dalta). The person is about 1.6 m high in scale. (d), A fining-upward fluvial cycle in unit 3 of the Hongyanangou section. The hammer is about 0.35 m long in scale.

subangular and poorly to moderately rounded grains suggest nearby source areas. In addition, in the Chengqiang section, the intermediate–acidic rocks are more abundant in units 1 and 2 than unit 3, whereas sedimentary and intermediate–basic clasts are more abundant in unit 3 than units 1 and 2. In the Hongyanangou section, more sedimentary clasts are present in unit 3 than units 1 and 2 and more intermediate–basic magmatic clasts are present in unit 2 than units 1 and 3. The andesite and dolerite clasts are similar in composition and type to the Middle Jurassic Tiaojishan Formation volcanic rocks (mainly andesite, with some basalt and tuff) to the southwest of the Liuleng Mountains, the middle of Fenghuang Mountains, and the basement of southern Yuxian Basin. The basalt clasts are similar to the Paleogene basalts in the Liuleng Mountains. The rhyolite and tuff clasts are similar to the Late Jurassic Donglingtai Formation in the south of the Fenghuang Mountains. Sandstones can be found in the basement of the basin but are primarily concentrated around the Yuxian Basin.

5.3 Detrital heavy minerals in the Chengqiang section

The heavy and light minerals in the Chengqiang section are predominantly angular to subangular. Ilmenite (4.57% –28.1%), limonite (7.4%–43.5%), and magnetite (6.41%–33.99%) are abundant detrital minerals in this section (Fig. 5). Pyroxene (2.4%–23.94%), amphibole (0.19%–27.6%), and garnet (1.26%–21.06%) are the most unstable minerals, and their content is highly variable in the section.

Magmatic zircons (0.13%–1.78%) are angular to subangular and idiomorphic (>85%). Wang et al. (2003) reported apatite (0.33%–5.29%), zircon (0.13%–1.78%), rutile (0%–1.15%), leucoxene (0%–1.53%), tourmaline (0%–0.02%), anatase (0%–0.46%), and titanite (0%–2.37%) mainly from acidic magmatic rocks. Thus, the sediments of unit 1 are mainly derived from acidic magmatic rocks (Fig. 4a). Epidote (0.57%–5.23%), pyroxene (0%–24.1%), amphibole (0.19%–27.6%), garnet (1.26%–21.06%), and some apatite and zircon grains are concentrated in unit 3, suggesting intermediate–basic volcanic rocks as a source. The variable mineral content of unit 2 suggests that it is a mixture of different types of magmatic rocks.

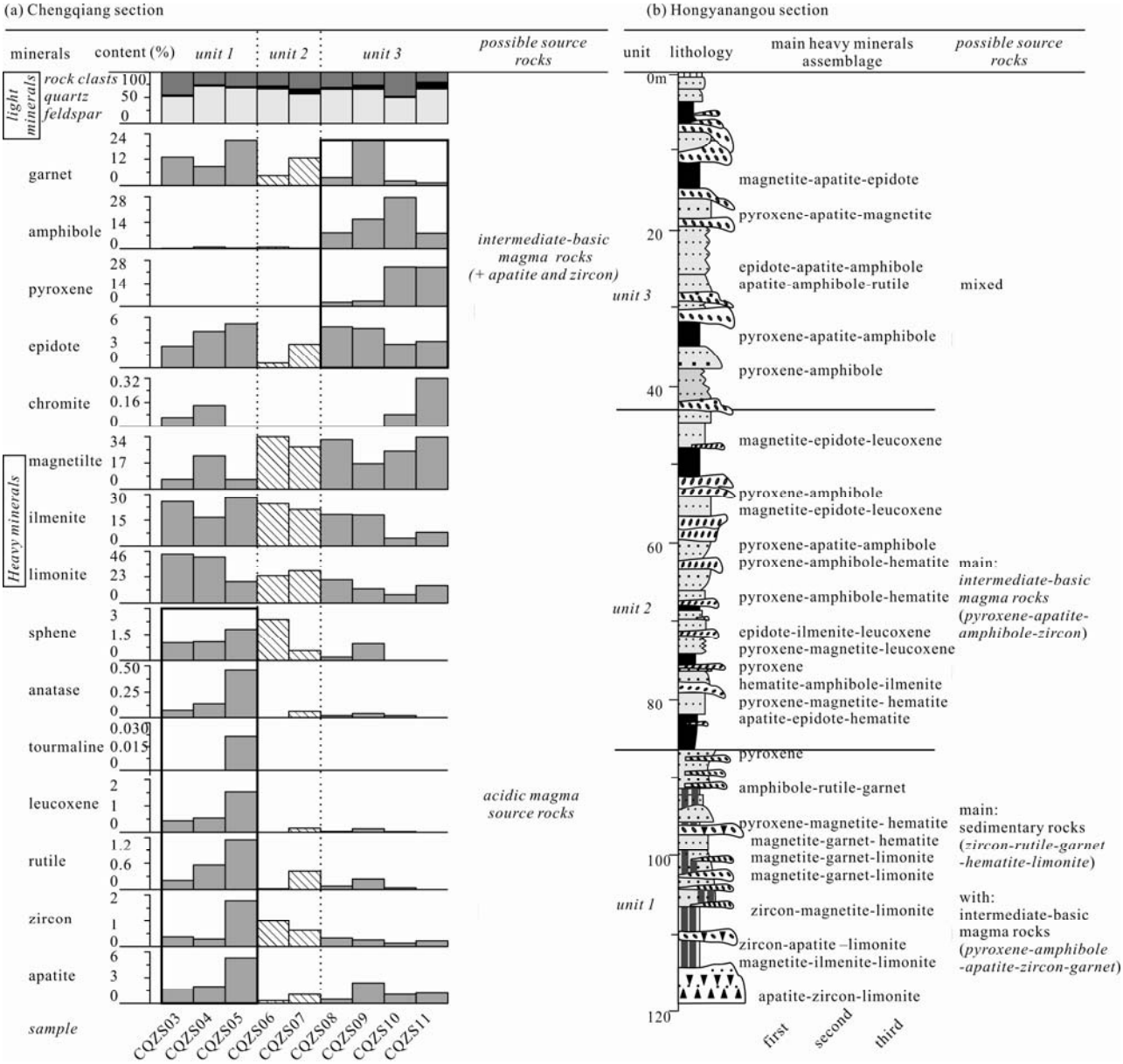

Fig. 5. (a) Bar char of the statistical detrital heavy minerals (DHM) from the Chengqiang section. (b) Major DHM assemblages of the Hongyanangou section (Chen, 1988).

5.4 Geochemistry of mud and silt in Chengqiang section

5.4.1 Major elements

Samples from the Chengqiang section have SiO_2 and Al_2O_3 ranging from 47.0–57.0 and 8.49–13.53 wt%, respectively (Table 1). K_2O content is between 1.8 and 2.88 wt%, and Na_2O is between 0.97 and 2.25 wt%. According to Pettijohn et al., 1987, the samples represent greywacke (9), litharenite (2), and arkose (1) (Fig. 6a). On the SiO_2/Al_2O_3 and $Fe_2O_3^T/K_2O$ classification diagram of Herron (Herron, 1988), almost all the analyzed sediments are classified as unstable immature wacke and only one as shale (Fig. 6b). The geochemical classification broadly coincides with the petrography observations.

5.4.2 Trace elements

The concentrations of trace elements are listed in Table 2. Compared with the Post-Archean Australian Shale (PAAS) (Taylor and McLennan, 1985), the contents of Cs (4.87–10.4 ppm), Ba (406–579 ppm), Rb (73.8–106 ppm), Sr (221–451 ppm, except Cqdh–10 on 912 ppm), and Sc (9.85–15.5 ppm) are high and similar to PAAS. All LILEs are similar throughout the section. Generally, all samples in the section show high concentration on Zr (103–163 ppm), Hf (3.29–5.48 ppm), Nb (10.2–15.9 ppm), and Ta (0.816–1.25 ppm). In all the samples, Zr–Hf and Nb–Ta are strongly correlated, with R^2 = 0.92 and 0.78, respectively. Co (8.31–17.3 ppm), Ni (19.1–39.9 ppm), and V (63.1–95.3 ppm) vary, whereas Cr (51.6–86.4

Table 1 Major element concentrations (wt%) for silts and mud of the Chengqiang section

unit	unit 1			unit 2			unit 3					
sample	Cqdh-01	Cqdh-02	Cqdh-03	Cqdh-04	Cqdh-05	Cqdh-06	Cqdh-07	Cqdh-08	Cqdh-09	Cqdh-10	Cqdh-11	Cqdh-12
rock type	silts	silts	mud	mud	silts	silts	mud	silts	silts	silts	silts	silts
SiO_2	47.36	54.33	48.47	49.59	57.75	55.68	53.16	49.17	55.64	53.86	56.43	47.59
Al_2O_3	9.81	11.27	11.01	13.53	12.3	12.91	11.37	10.33	11.39	12.06	10.59	8.49
$Fe_2O_3^T$	3.89	3.34	3.74	4.61	4.34	4.77	4.08	3.88	4.26	4.3	3.91	2.5
MgO	3.06	3.05	2.95	3.41	2.81	3.06	3.28	5.52	4.66	3.05	4.13	6.47
CaO	14.6	9.98	13.31	9.63	7.72	7.42	10.33	11.3	7.44	9.27	8.55	12.77
Na_2O	0.965	1.43	1.39	1.16	1.8	1.64	1.69	1.51	1.9	2.25	1.79	1.88
K_2O	2.3	2.61	2.38	2.88	2.51	2.66	2.46	2.06	2.32	2.51	2.13	1.8
MnO	0.17	0.04	0.07	0.05	0.11	0.11	0.08	0.08	0.07	0.06	0.08	0.08
TiO_2	0.58	0.61	0.59	0.67	0.60	0.64	0.63	0.57	0.62	0.65	0.59	0.43
P_2O_5	0.12	0.11	0.11	0.10	0.15	0.14	0.14	0.15	0.13	0.15	0.13	0.10
LOI	16.95	13.04	15.76	14.19	9.91	10.90	12.72	15.15	11.30	11.72	11.38	17.81
FeO	0.79	1.11	1.09	1.01	1.00	0.79	1.08	1.24	1.32	0.93	1.81	1.08
SiO_2/Al_2O_3	4.83	4.82	4.40	3.67	4.70	4.31	4.68	4.76	4.89	4.47	5.33	5.61
Na_2O/K_2O	0.42	0.55	0.58	0.40	0.72	0.62	0.69	0.73	0.82	0.90	0.84	1.04
$Fe_2O_3^T/K_2O$	1.69	1.28	1.57	1.60	1.73	1.79	1.66	1.88	1.84	1.71	1.84	1.39
Al_2O_3/TiO_2	17.03	18.54	18.69	20.28	20.63	20.05	17.96	18.28	18.37	18.61	17.92	19.74
K_2O/Na_2O	2.38	1.83	1.71	2.48	1.39	1.62	1.46	1.36	1.22	1.12	1.19	0.96

Note: LOI, loss on ignition.

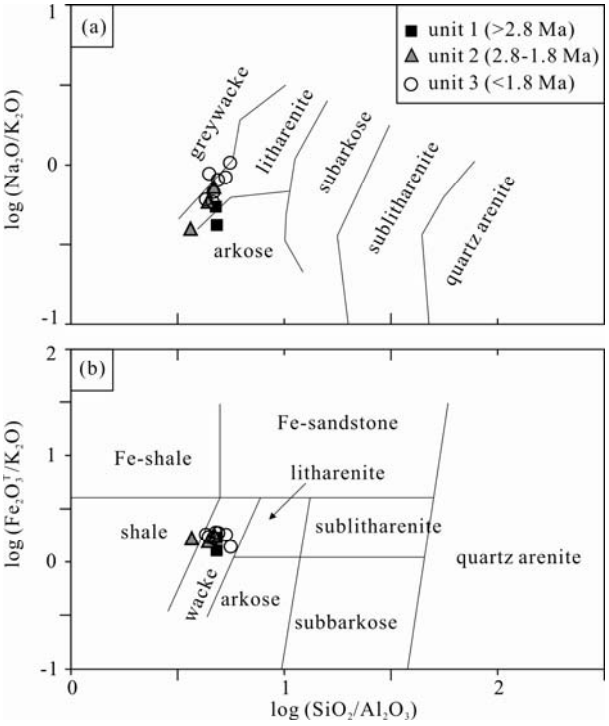

Fig. 6. Chemical classification diagram discriminating siliciclastic sediments by their logarithmic ratios of (a) SiO_2/Al_2O_3 versus Na_2O/K_2O (after Pettijohn et al. 1987) and (b) $Fe_2O_3^T/K_2O$ (after Herron 1988).

ppm), Sc (9.85–15.5 ppm) and Cr/Ni (1.79–2.71), Ni/Co (2.05–2.75), Sc/Ni (0.33–0.52), and Sc/Cr (0.16–0.21) are similar to UCC in the entire section. Furthermore, the averages are normalized to the average UCC (Fig. 7a) (Taylor and McLennan, 1985). Several deviations from the UCC values are observed; these values include negative Sr, P, Ba, Zr, and Nb anomalies; positive U, Cs, and V–Cr–Ni anomalies; and slightly positive Yb–Ti anomalies.

5.4.3 Rare earth elements (REE)

Total REE (ΣREE) values in the Chengqiang section are nonvariable (Table 3). All samples exhibit light REE (LREE)-enriched chondrite-normalized patterns, similar to UCC and PAAS (Figs. 7c and 7d), LREE enrichment (high (La/Sm)cn, (La/Yb)cn, and ΣLREE/ΣHREE), flat HREE ((Gd/Yb)cn = 1.30–1.50, average 1.40), and significant negative Eu anomalies (Eu/Eu*, typically 0.61–0.68). The total REE in different units are similar, and there are no systematic differences in the REE among the different stratigraphic units (Figs. 7c and 7d). ΣREE/Al ranges from 12.26 to 18.18, which is higher than UCC (9.68; Taylor and McLennan, 1985), suggesting that nonclay detrital phases significantly contribute to the ΣREE content of the clastic sediments in the section (Singh and Rajamani, 2001; López et al., 2005). However, Zr shows moderate correlation with ΣREE, ΣLREE, and ΣHREE (R^2 = 0.55, 0.52, and 0.69, respectively), suggesting that the zircon in the heavy minerals has affected the total REE probably because it is largely controlled by irregular distribution during sedimentation (López et al., 2005).

6 Discussion

6.1 Source areas

6.1.1 Source-rock composition of the Chengqiang section from the geochemistry

Multi-element spider diagrams are effective indicators of the tectonic environment and source-rock composition. On the UCC-normalized spider diagram proposed by Floyd et al. (Floyd et al., 1991), the samples from the Chengqiang section have high Cs and V–Cr–Ni contents and low Nb and Zr contents (Fig. 7a). Apparently, there is a small contribution from mature sedimentary detritus in

Table 2 Trace element concentrations (ppm) for silts and mud of the Chengqiang section

unit	unit 1			unit 2			unit 3					
sample	Cqdh-01	Cqdh-02	Cqdh-03	Cqdh-04	Cqdh-05	Cqdh-06	Cqdh-07	Cqdh-08	Cqdh-09	Cqdh-10	Cqdh-11	Cqdh-12
rock type	silts	silts	mud	mud	silts	silts	mud	silts	silts	silts	silts	silts
Li	28.4	27.3	30.7	39.4	38.3	33.8	36	32.7	50.4	45.5	35.5	26.2
Be	1.89	1.43	1.71	1.98	2.43	1.59	1.68	1.4	2.31	2.03	1.83	1.64
Sc	10.9	9.85	10.7	15.3	13	12.5	12.2	10.4	15.5	14.9	11.6	10
V	80.1	67	74.4	89.5	69.4	79.6	77.6	80.5	94.6	95.3	76	63.1
Cr	51.6	51.7	58.9	89	70.7	65.2	66.7	58.8	86.4	81.6	73.1	53.1
Co	11.7	8.31	11.4	13.4	14.7	17.3	15	12.4	17.1	14.8	15.5	12.2
Ni	27.2	19.1	27.6	36.8	35.4	36.5	30.7	33.7	39.9	39.1	35.3	26.9
Cu	27.9	15.5	21.9	32.5	24.2	24.6	21.8	22.7	26.4	29	21.8	31.8
Zn	70	52.4	58.6	77.4	74.7	71.6	65.8	66.3	80.1	83.6	61.8	62.3
Ga	12	12.7	13.8	15.9	15.4	15.1	14	13.6	16.9	15.9	13.1	11.4
Rb	90.9	85.4	85.2	105	99.8	91.7	91.5	80.3	106	104	84.7	73.8
Sr	228	221	268	245	281	234	311	451	376	912	360	405
Y	24.6	18.1	22.1	21.5	22.2	19.5	22.7	20.6	27.2	26.7	22.1	19.4
Zr	126	117	125	112	125	109	136	119	163	141	141	103
Nb	13.3	13.1	13.2	13.3	14.2	12.4	13.3	11.8	15.9	14.4	12.8	10.2
Cs	6.63	6.33	7.29	10.4	7.73	7.34	7.31	5.5	8.02	8.8	6.31	4.87
Ba	406	456	452	437	484	457	525	579	570	597	521	525
Hf	3.98	3.93	4.32	3.97	4.57	3.56	4.62	3.82	5.48	4.73	4.77	3.29
Ta	1.04	0.98	1.15	1.15	1.24	0.95	1.15	0.82	1.25	1.21	1.03	0.82
Tl	0.55	0.59	0.58	0.72	0.62	0.59	0.57	0.47	0.67	0.64	0.52	0.49
Pb	20.6	18.9	20.5	18.3	24.6	20.4	20.8	18.5	23.4	23.5	18.6	18.4
Bi	0.33	0.24	0.28	0.30	0.29	0.29	0.28	0.25	0.30	0.33	0.26	0.18
Th	8.83	8.79	9.42	10.6	9.99	9.05	9.43	8.62	11.2	11.3	8.91	6.9
U	5.14	4.97	4.67	2.58	2.9	5.5	3.34	6.47	6.83	5.11	3.21	3.68
Cr/Ni	1.90	2.71	2.13	2.42	2.00	1.79	2.17	1.75	2.17	2.09	2.07	1.97
Ni/Co	2.33	2.30	2.42	2.75	2.41	2.11	2.05	2.72	2.33	2.64	2.28	2.21
Sc/Ni	0.40	0.52	0.39	0.42	0.37	0.34	0.40	0.31	0.39	0.38	0.33	0.37
Sc/Cr	0.21	0.19	0.18	0.17	0.18	0.19	0.18	0.18	0.18	0.18	0.16	0.19
Th/Sc	0.81	0.89	0.88	0.69	0.77	0.72	0.77	0.83	0.72	0.76	0.77	0.69
Zr/Sc	11.56	11.88	11.68	7.32	9.62	8.72	11.15	11.44	10.52	9.46	12.16	10.30
Cr/Th	5.84	5.88	6.25	8.40	7.08	7.20	7.07	6.82	7.71	7.22	8.20	7.70
Co/Th	1.33	0.95	1.21	1.26	1.47	1.91	1.59	1.44	1.53	1.31	1.74	1.77

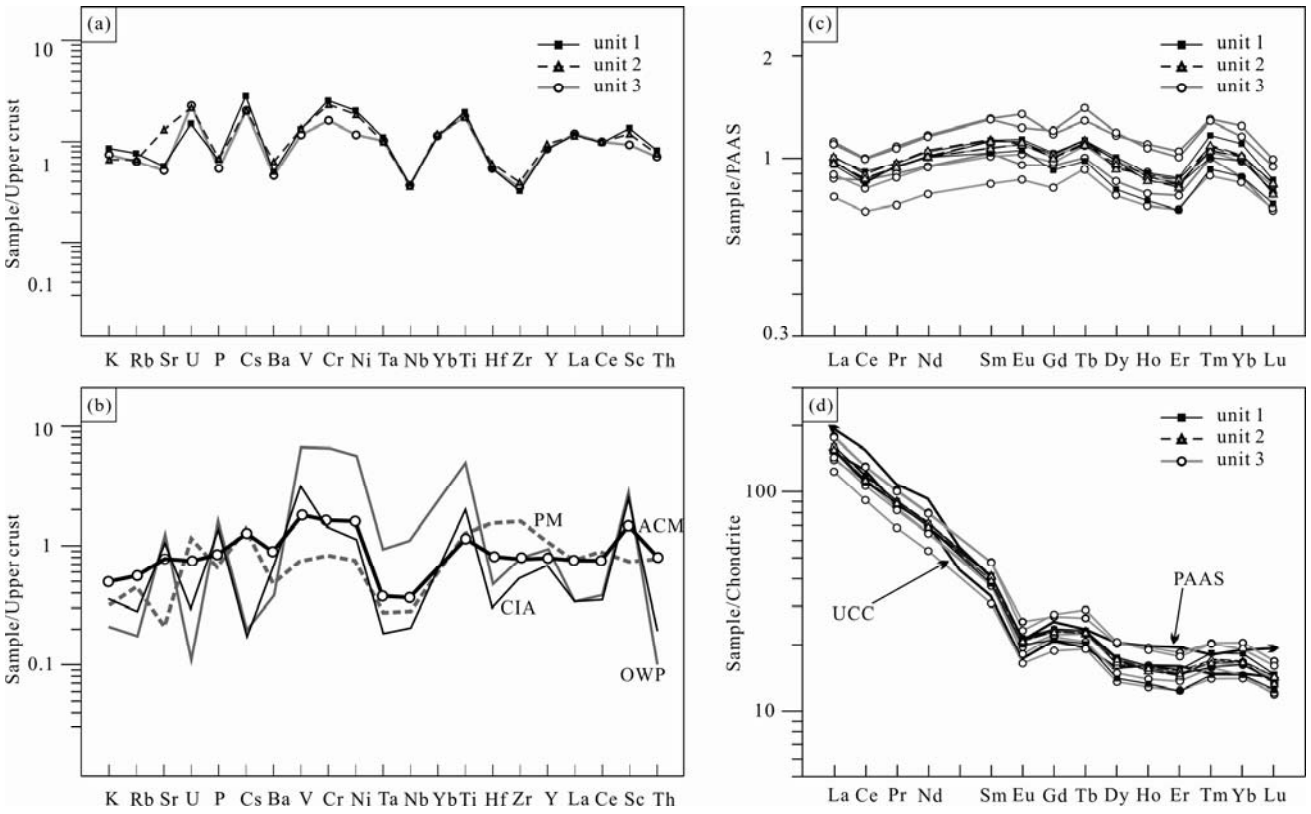

Fig. 7. Spider diagrams and REE patterns of Formation averages for the Chengqiang section.

(a), Normalized to average upper continental crustal values (after Floyd et al. 1991). (b), Expected values for comparison for passive margin (PM), active continental margin + continental island arc (ACM), oceanic within-plate (OWP), and continental island arc (OIA) settings. (c) REE normalized to PAAS and (d) to chondrite (after Taylor and McLennan 1985).

Table 3 Rare earth element concentrations (ppm) for silts and mud of the Chengqiang section

unit	unit 1			unit 2			unit 3					
sample	Cqdh -01	Cqdh-02	Cqdh-03	Cqdh-04	Cqdh-05	Cqdh-06	Cqdh-07	Cqdh-08	Cqdh-09	Cqdh-10	Cqdh-11	Cqdh-12
rock type	silts	silts	mud	mud	silts	silts	mud	silts	silts	silts	silts	silts
La	38.20	37.30	36.30	38.50	36.80	34.80	37.00	33.10	42.50	41.80	34.00	29.30
Ce	73.00	68.20	67.30	71.70	69.80	64.20	69.30	68.80	80.00	79.50	65.10	55.90
Pr	8.59	8.37	8.45	8.64	8.38	7.73	8.42	8.01	9.65	9.51	7.80	6.49
Nd	33.40	32.20	32.20	33.80	32.50	29.80	32.30	30.30	37.40	37.00	30.10	25.10
Sm	6.33	5.80	6.28	6.37	6.29	5.72	6.01	5.79	7.31	7.26	5.67	4.71
Eu	1.25	1.16	1.23	1.21	1.23	1.10	1.21	1.05	1.48	1.35	1.13	0.95
Gd	4.87	4.33	4.81	4.86	4.71	4.31	4.73	4.47	5.53	5.66	4.57	3.85
Tb	0.87	0.76	0.87	0.87	0.85	0.76	0.85	0.77	0.99	1.08	0.84	0.71
Dy	4.43	3.56	4.32	4.10	4.23	3.78	4.35	3.76	5.13	5.23	4.14	3.43
Ho	0.90	0.75	0.86	0.89	0.86	0.75	0.88	0.79	1.10	1.07	0.91	0.73
Er	2.54	2.04	2.42	2.51	2.38	2.18	2.43	2.25	3.04	2.92	2.44	2.05
Tm	0.47	0.37	0.40	0.43	0.44	0.38	0.42	0.40	0.52	0.51	0.42	0.36
Yb	3.09	2.47	2.75	2.84	2.86	2.53	2.83	2.46	3.48	3.24	2.74	2.38
Lu	0.37	0.32	0.34	0.36	0.36	0.30	0.34	0.30	0.43	0.41	0.36	0.31
ΣREE	178.30	167.6	168.5	177.1	171.7	158.3	171.1	162.3	198.6	196.5	160.2	136.3
L REE	160.80	153.0	151.8	160.2	155.0	143.4	154.2	147.1	178.3	176.4	143.8	122.5
H REE	17.54	14.59	16.77	16.87	16.69	14.98	16.84	15.20	20.22	20.12	16.41	13.81
LREE/HREE	9.17	10.49	9.05	9.50	9.29	9.57	9.16	9.67	8.82	8.77	8.76	8.86
Eu/ Eu*	0.66	0.68	0.66	0.64	0.66	0.65	0.67	0.61	0.68	0.62	0.66	0.66
La/Sc	3.51	3.79	3.39	2.52	2.83	2.78	3.03	3.18	2.74	2.81	2.93	2.93
La/Th	5.98	4.35	3.96	3.43	3.85	4.07	3.69	4.29	2.96	3.76	4.69	4.93
$(La/Sm)_{cn}$	3.90	4.15	3.73	3.90	3.78	3.93	3.97	3.69	3.75	3.72	3.87	4.02
$(La/Yb)_{cn}$	8.87	10.83	9.47	9.72	9.23	9.87	9.38	9.65	8.76	9.25	8.90	8.83
$(Gd/Yb)_{cn}$	1.30	1.45	1.45	1.42	1.36	1.41	1.38	1.50	1.32	1.45	1.38	1.34

Note: cn, chondrite normalization.

the section. The negative Sr anomalies in units 1 and 2 are typical of old recycled environments and passive continental margins (Floyd et al., 1989). Comparing the average values of units 1, 2, and 3 to PM, ACM, OIA, and OWP settings (Fig. 7b), we find that the spider diagrams of the clastics better agree with continental island arc or active continental margin settings (units 2 and 3), suggesting the presence of dacite to granodiorite source rocks.

The REE and Eu of sedimentary rocks are the most reliable indicators of provenance (Bhatia, 1985; Taylor and McLennan, 1985; McLennan, 1989) because their elemental distributions are strongly affected by sedimentary processes, diagenesis, and metamorphism (Bhatia and Crook, 1986; McLennan and Taylor, 1991; Condie, 1993). The significant LREE enrichment and flat HREE patterns of the clastics in the Chengqiang section (Table 3 and Fig. 7d) suggest that the sources rocks were chiefly felsic, and the distinctive negative Eu anomaly is evidence for a differentiated source, similar to granite or rhyolite. The Eu anomalies in all samples (0.61–0.68, average 0.65; Table 3) are similar to the average value of 0.65 for craton-derived PAAS (Fig. 7d).

The ratios of some elements, such as SiO_2/Al_2O_3, K_2O/Na_2O, Th/Sc, La/Sc, Zr/Sc, Co/ Th, Cr/Th, Cr/V, and Eu/ Eu*, are particularly sensitive to average source compositions (Bhatia, 1985; Taylor and McLennan, 1985; Girty et al., 1996). These ratios are most diagnostic for differentiating felsic from mafic source components and are not affected by dilution (Taylor and McLennan, 1985; Bhatia and Crook, 1986). The $(SiO_2/20) - (Na_2O + K_2O) - (MgO + TiO_2 + FeO^*)$ diagram (Hayashi et al., 1997), and the SiO_2/Al_2O_3 and K_2O/Na_2O vs ΣREE relations (Bhatia, 1985) suggest that the sediments in units 1 and 2

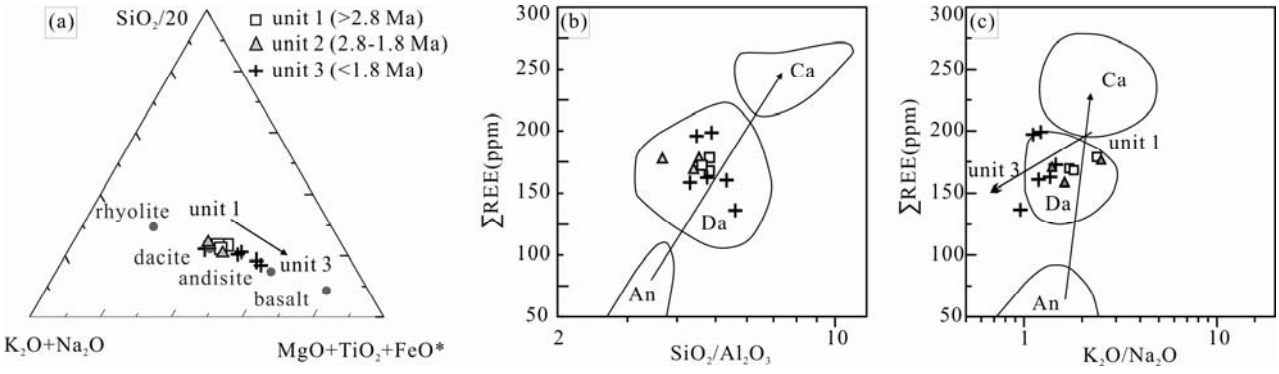

Fig. 8. Discrimination diagrams illustrating provenance rocks of the sediments.
(a), $(SiO_2/20)$-(Na_2O+K_2O)-$(MgO+TiO_2+FeO^*)$ diagram (after Hayashi et al. 1997). (b) SiO_2/Al_2O_3 vs. ΣREE relationship and (c) K_2O/Na_2O vs. ΣREE relationships (after Bhatia, 1983). Components: An, andesitic source rocks; Da, dacitic source rocks; Ca, Granite-gneiss and sedimentary source rocks.

are mainly derived from dacitic source rocks, whereas unit 3 are derived from dacitic and andesite source components (Figs. 8a–8c). In addition, the Al_2O_3/TiO_2 ranges from 17.03–20.64 (average 18.84), suggesting that they are derived from felsic igneous rocks (Girty et al., 1996).

The Th/Sc and La/Sc ratios of unit 1 (0.69–0.89 and 2.52–3.79, respectively; Tables 2 and 3) show characteristics between continental island arc (0.85 and 1.82, respectively) and active continental margin (2.59 and 4.55, respectively) settings (Bhatia and Crook, 1986). However, in unit 2 (0.69–0.72 and 2.52–2.83, respectively) and unit 3 (0.69–0.83 and 2.74–3.03, respectively), they are lower than unit 1 and more characteristic of continental island arc setting (Bhatia and Crook, 1986). This suggests that the felsic components are dominant in the source rocks of all samples, but there are sufficient contributions from mafic components in units 2 and 3. This is consistent with the higher contents of Co, Cr, Ni, Sc, and V in units 2 and 3 (Table 3). In addition, the average Th/Sc in unit 1 (0.86) is similar with the values in PAAS and UCC (0.9) (Taylor and McLennan, 1985), whereas the values in unit 2 (0.73) and unit 3 (0.76) are lower. Therefore, when plotted on the Zr/Sc–Th/Sc diagram (Fig. 9a), unit 1 is more close to the UCC than units 2 and 3. This also suggests a relatively felsic source rock for the Chengqiang section but with more mafic components for units 2 and 3. The Cr/Th and Eu/Eu* values (3.1–7.6 and 0.59–0.87, respectively) also fall in the felsic range (2.5–17.5 and 0.48–0.78, respectively), as suggested by Cullers (Cullers, 1994). Floyd and Leveridge (Floyd and Leveridge, 1987) established a discrimination diagram using the La/Th vs. Hf to determine different arc components and sources (Fig. 9b). Uniformly low La/Th (2.96–5.98) and Hf (3.56–4.77 ppm) in the samples suggest their derivation predominantly from a felsic arc source, i.e., typical granites and granodiorites (Gill, 1981). The samples have low Co/Th (0.95–1.77) and high La/Sc (2.52–3.78), suggestive of predominantly felsic volcanic rocks (Fig. 9c; Taylor and McLennan, 1985). All features suggest mixed, multiple-sourced sediments, including felsic and mafic components for the sediments of the Chengqiang section. The felsic components in unit 1 are more dominant than in units 2 and 3.

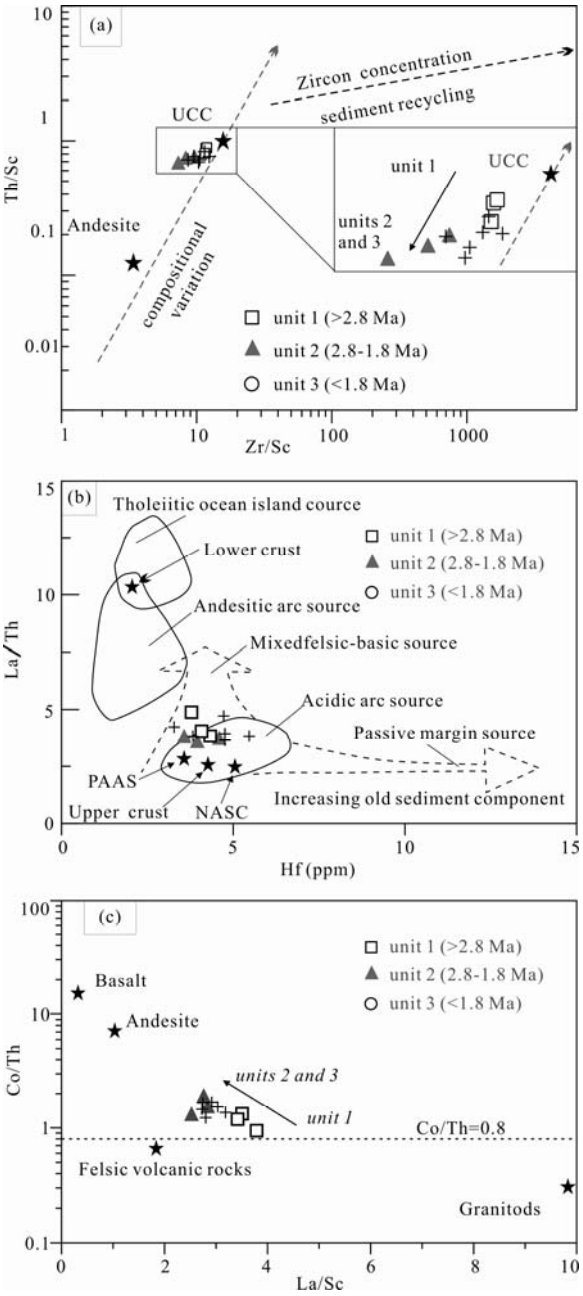

Fig. 9. Discrimination diagrams illustrating sediment recycling and provenance.
(a), Th/Sc vs. Zr/Sc diagram (after McLennan et al. 1993). (b), La/Th vs. Hf diagram (after Floyd and Leveridge 1987). PAAS and UCC values are from Taylor and McLennan (1985), and the NASC value is from Gromet et al. (1984). (c), La/Sc-Co/Th diagram (after Taylor and McLennan 1985).

6.1.2 Source areas of both sections

In both Chengqiang and Hongyanangou sections, the poorly sorted, poorly rounded, and angular or subangular clasts and the angular to subangular sands suggest that these sediments were shed from a nearby provenance. Low-maturity deposits with high feldspar content (Fig. 5a) and the dominance of greywacke, litharenite (Fig. 6a), and wacke (Fig. 6b) in the fine clastics support this deduction.

Because different rocks weather differently, different rock assemblages are preserved in varied grains. Thus, the heavy minerals suggest intermediate to acidic magmatic and mixed intermediate to basic magmatic components in units 1–3 of the Chengqiang section (Fig. 5a), whereas the coarse clasts (Fig. 3a) and geochemistry suggest intermediate to basic magmatic and intermediate to acidic magmatic components in this section, respectively.

Nevertheless, unit 1 has more intermediate to acidic magmatic components than units 2 and 3. Combined with the paleocurrents and geological map, we infer that the main source areas of the Chengqiang section changed from the south of the Fenghuang Mountains in unit 1 (rhyolite and tuff) to the north of the Fenghuang Mountains in unit 2 (sedimentary rocks), then to middle of the Fenghuang Mountains (basalt, andesite, and dolerite), and the Yuxian Basin (sedimentary rocks) in unit 3 (Fig. 1d).

In the Hongyanangou section, the clasts comprise intermediate to basic magmatic rocks, even with some intermediate to acidic rocks in unit 1 and sedimentary rocks in unit 3 (Fig. 3b). This is consistent with the heavy minerals reported by Chen (1988). Considering the paleocurrent data in this study (Fig. 3b) and the heavy minerals (Fig. 5b) , the source areas of the Hongyanangou section are probably north of the Fenghuang Mountains in unit 1, south of the Liuleng Mountains in unit 2, and the Liuleng Mountains and Yuxian Basin in unit 3.

6.2 Basin evolution model

Based on data for the middle (Chen et al., 2012; Min et al., 2015) and northern part (Chen, 1988; Chen et al., 2015), and for the southern part of the basin, a cross section from south to north is shown in Fig. 10. In the cross section, the differences in provenance and sedimentary environments between the middle to northern and southern parts are remarkable. The mid-northern area evolved from deep water in Pliocene to shallow water environment in Pleistocene. The Chengqiang and Hongyanangou sections in the south, however, experienced diametrically opposite evolution with deepening-upward water environment during the same era. Therefore, the basin is divided into two parts by the Liulengshan Fault, with the main geotectogene in the mid-northern part and a subgeotectogene in the southern part (Fig. 1c). The differences in evolution are consistent with the regional stress regime proposed by Shi et al. (2015). Thus, the following relation between the evolution of the basin and faulting is proposed.

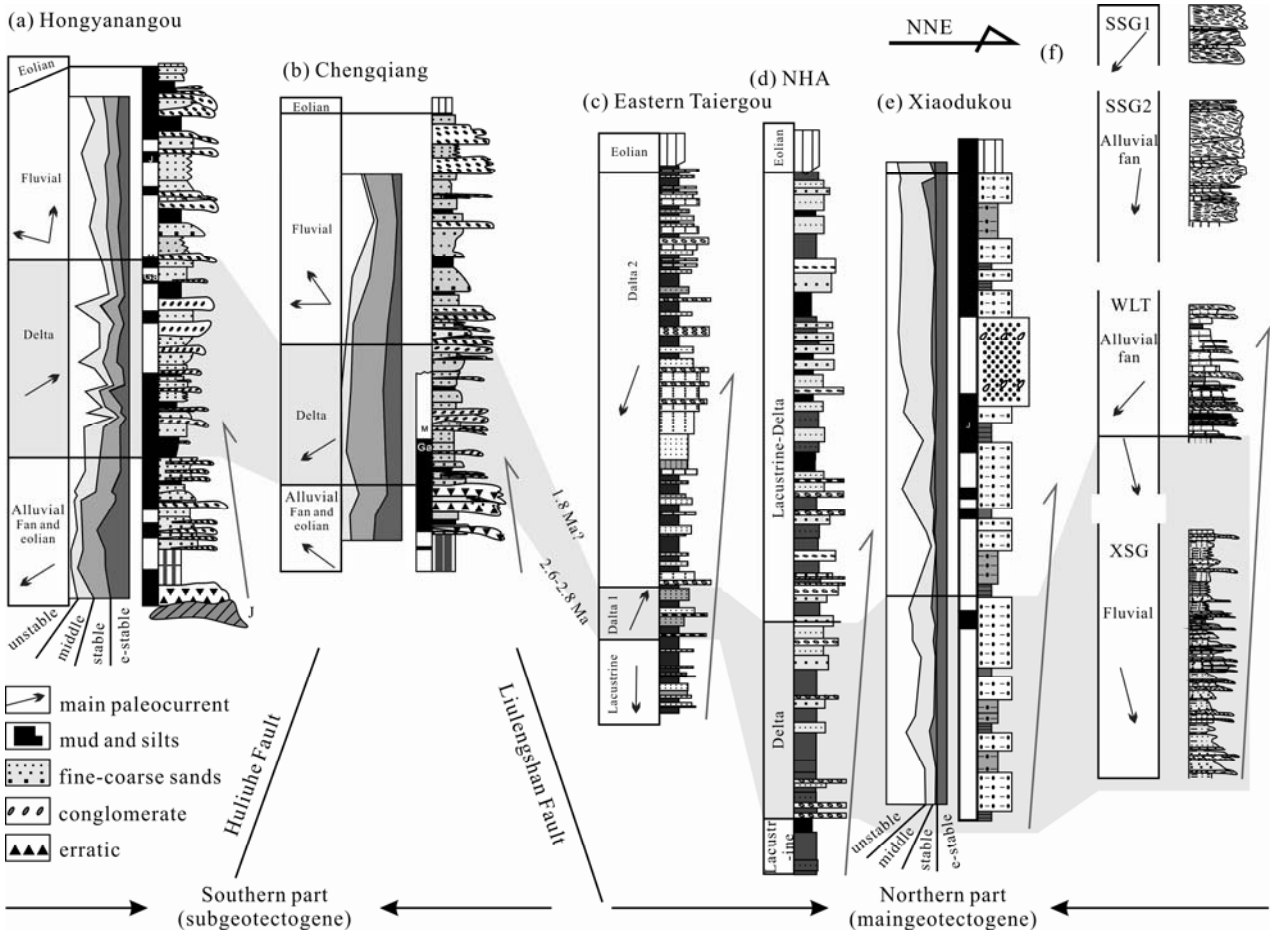

Fig.10. The cross section based on different sections from south to north in the Nihewan Basin.
Ages of the (a) Hongyanangou section is from Chen (1988), and (b) Chengqiang section is from Li and Wang (1982) and Du et al. (1995), (c) Eastern Taiergou is from Chen et al. (2012), (d) NHA is from Min et al., (2015), (e) Xiaodukou is from Chen (1988), and XSG, WLT, SSG1 and SSG2 are from Chen et al. (2015).

6.2.1 Before ~2.8–2.6 Ma

In the mid-northern part, affected by the NW–SE transtensional stress regime (Shi et al., 2015b), the normal Liulengshan Fault was active (Fig. 11a) and the basin underwent rapid NW–SE extension during the Pliocene (before ~2.6 Ma). The main geotectogene, represented by the Eastern Taiergou section (Chen et al., 2012, 2015) and NHA core (Min et al., 2015), was a lacustrine environment. The paleocurrent in the Eastern Taiergou section shows sediment derivation from the northern Xiong'er Mountains (Chen et al., 2015). In the southern part, deposition is much different. The alluvial fan and eolian sediments were deposited in a temporary depression at depth of 20–30 m (unit 1 of the two sections), much less

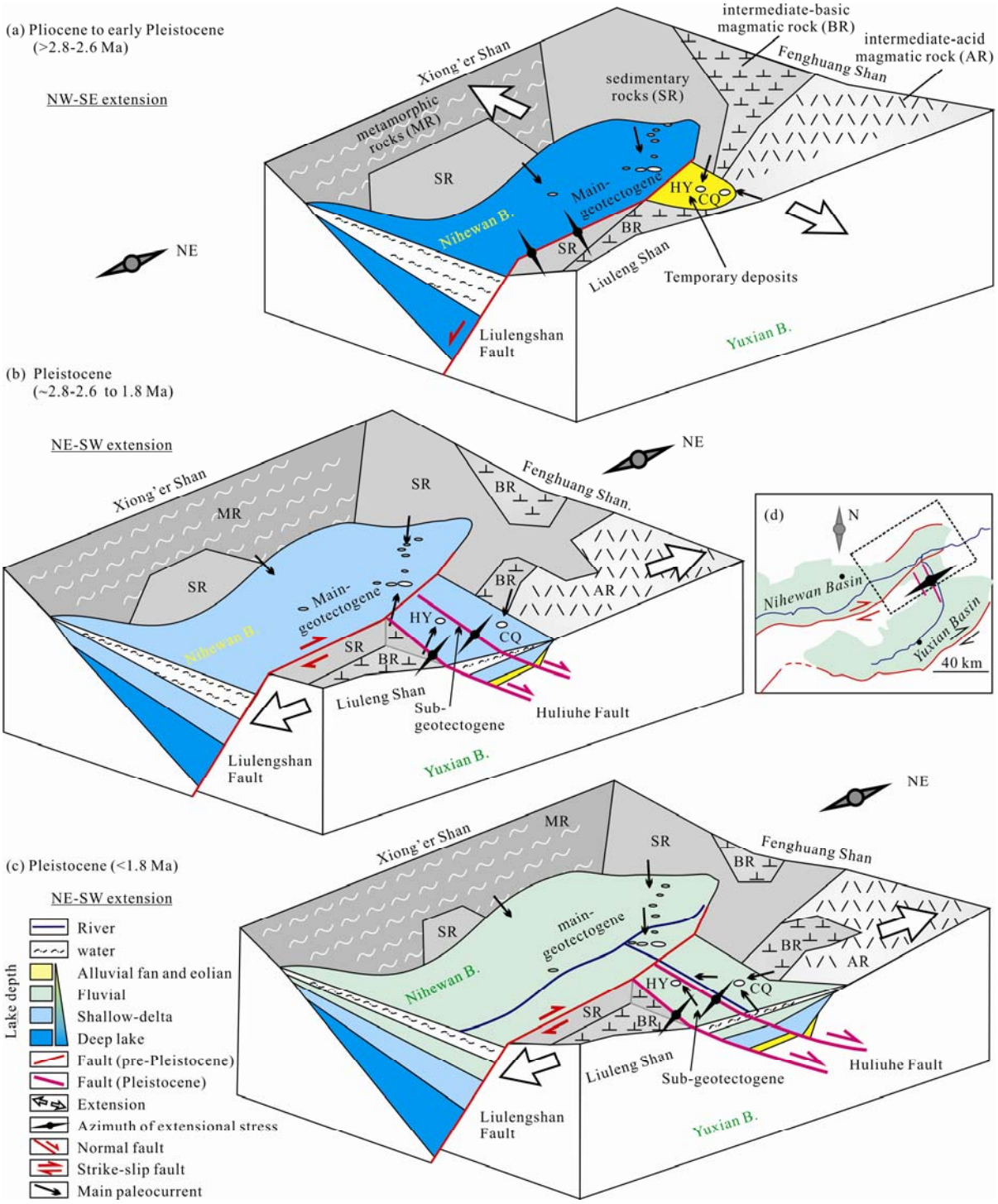

Fig.11. (a), (b) and (c) Schematic map showing evolution model of a main-geotectogene in the middle-northern part of the Nihewan Basin and a sub-geotectogene in the southern part. The evolution was controlled by the regional regime shift suggested by Shi et al. (2015b). (d) Regional regime state of the third stage (c).

than the ~220 m thick lacustrine sediments in the mid-northern parts (Min et al., 2015). The paleocurrents, clast components, heavy minerals, and chemistry data suggest that the unit 1 sediments in the Chengqiang and Hongyanangou sections mainly originated from the south and north of the Fenghuang Mountains. It is possible that these two sections were near Fenghuang Mountains at this stage.

6.2.2 From ~2.8–2.6 Ma to ~1.8 Ma

In Early Pleistocene (from ~2.8–2.6 Ma to ~1.8 Ma), the regional regime was NE–SW extension (Shi et al., 2015b), represented by the strike-slip Liulengshan Fault and normal Huliuhe Fault. Consequently, the sedimentary environment and provenance changed in the mid-northern and southern parts. Because of the strike-slip Liulengshan Fault, the accommodation space of the mid-northern part decreased sharply. Delta facies replaced the lacustrine facies in the Eastern Taiergou section (Chen et al., 2012) and NHA core (Min et al., 2015). The paleocurrents shifted to south (Liuleng Mountains) in the Eastern Taiergou section and northwest in the Xiashagou area (Chen et al., 2015). Such rapid increase in the accommodation space in the southern part might result from the activity of the Huliuhe Fault. As for the subgeotectogene, it formed in the Chengqiang–Hongyanangou area and was dominated by fan delta deposits and abundant *Ostracoda* (Chen, 1988). The main source area of the sections changed to the middle of the Fenghuang Mountains and southeast of the Liuleng Mountains. The increased sediment contribution from the Liuleng Mountains in the mid-northern (Eastern Taiergou section) and southern (Hongyanangou section) parts is related to the rapid uplift of the Liuleng Mountains and the active Huliuhe Fault.

6.2.3 After ~1.8 Ma

After ~1.8 Ma, the alluvial fan and delta sediments were eroded from the Xiong'er Mountains and replaced by fluvial and delta deposits in the mid-northern part. In the southern part, the paleocurrents shifted to the north (Yuxian Basin) and the fluvial deposits replaced the fan delta sediments. The paleo-Huliuhe River, which connected the two basins, could be responsible for this shift. The continuous material input from the surrounding mountains during the NW–SE weak extension decreased the accommodation space of the mid-northern part of the Nihewan Basin and the Yuxian Basin. The decreased accommodation space and the NE–SW extension of the Huliuhe Fault triggered the river formation.

In summary, the Nihewan Basin underwent a three-stage evolution in the Middle Pliocene–Pleistocene. The stages were controlled by NW–SE extension in Pliocene and the subsequent weaker NE–SW extension in Pleistocene, which were predominantly affected by the outward growth of the Tibetan Plateau (Shi et al., 2015b). The shift in the mid-northern and southern parts of the basin occurred at ~2.8–2.6 and ~1.8 Ma and corresponds to the data around the Ordos Block (Chen et al., 2016; Shi et al., 2015b).

7 Conclusions

(1) The Chengqiang and Hongyanangou sections in the southern Nihewan Basin comprise Pliocene–Pleistocene eolian and alluvial fan facies before ~2.8 Ma, fan delta in ~2.8–1.8 Ma, and fluvial after ~1.8 Ma.

(2) The main source rocks of the sections are Jurassic magmatic rocks from the Fenghuang Mountains and Liuleng Mountains, and partly from the Yuxian Basin, but the source areas varied in different stages.

(3) The temporal and spatial evolution of the sedimentation and source areas of the basin was controlled by the shift of the regional regime in the Shanxi Graben from the Pliocene NW–SE extension to the Pleistocene NE–SW extension.

Acknowledgements

This study was supported by Grants from National Natural Science Foundation of China (No. 41172150), the Ministry of Land and Resources of China (No. 201211005–1), China Geological Survey (CGS) (No. 1212011120099), and China Scholarship Council (CSC). We are grateful to acknowledge editors and anonymous reviewers for their critical, constructive comments to improve the manuscript, as well as Jinsong Yang for attending the field work.

Manuscript received Sept. 4, 2017
accepted Dec. 3, 2017
edited by Liu Lian

References

Allen, J.R.L., 1970. Studies in fluviatile sedimentation: a comparison of fining-upwards cyclothems, with special reference to coarse-member composition and interpretation. *Journal of Sedimentary Petrology*, 40(1): 298–323.

Bhatia, M.R., 1985. Rare earth element geochemistry of Australian Paleozoic graywackes and mudrocks: provenance and tectonic control. *Sedimentary geology*, 45(1): 97–113.

Bhatia, M.R., and Crook, K.A., 1986. Trace element characteristics of graywackes and tectonic setting discrimination of sedimentary basins. *Contributions to mineralogy and petrology*, 92(2): 181–193.

Cai Baoquan, Zheng Shaohua and Li Qiang, 2007. Plio-pleistocene small mammals from the Niutoushan section of the Yuxian Basin, China. *Vertebrata Palasiatica*, 45(3): 232–245 (in Chinese with English abstract).

Cande, S.C., and Kent, D.V., 1995. Revised calibration of the geomagnetic polarity timescale for the Late Cretaceous and Cenozoic. *Journal of Geophysical Research: Solid Earth*, 100 (B4): 6093–6095.

Cant, D.J., and Walker, R.G., 1976. Development of a braided-fluvial facies model for the Devonian Battery Point Sandstone, Quebec. *Canadian Journal of Earth Sciences*, 13 (1): 102–119.

Chen Guoda, 1987. On the geotectonic nature of the Fen-Wei rift system. *Tectonophysics*, 143(1–3): 217–223.

Cen Min, Dong Shuwen, Shi Wei, Zhou Taofa, Chen Long and Chen Xingqiang, 2015. Structural analysis on the formation mechanism of Datong Basin. *Geological Review*, 61(6): 1235–1247 (in Chinese with English abstract).

Chen Maonan, 1988. *Study on the Nihewan Beds*. Beijing: China Ocean Press, 143 (in Chinese).

Chen Xingqiang, Shi Wei, Hu Jianmin and Dong Shuwen, 2016. Sedimentation of the Pliocene-Pleistocene Chaizhuang section in the Central Linfen Basin, North China and its tectonic significance. *Journal of Geomechanics*, 22(4): 984–993 (in Chinese with English abstract).

Chen Xingqiang, Chi Zhenqing, Dong Shuwen, Yan Zhen, Yang Jinsong, Shi Wei, Min Longrui, Wang Yong and Yao Peiyi, 2015. Late Cenozoic sedimentation of Nihewan Basin, central North China and its tectonic significance. *Journal of Asian Earth Sciences*, 114: 242–257.

Chen Xingqiang, Chi Zhenqing, Yan Zhen, Wang Yong, Min Longrui, Yao Peiyi, Dong Jin and Yao Dulin, 2012. Features of sedimentary facies of the Nihewan Basin in North China: An example from the Eastern Taiergou section. *Earth Science Frontiers*, 19(4): 227–238 (in Chinese with English abstract).

Cheng Guoliang, Li Suling and Lin Jinlu, 1978. A preliminary paleomagnetic survey of the Nihewan Bed. *Scientia Geologica Sinica*, 7(3): 247–252 (in Chinese with English abstract).

Chi Zhenqing, Liu Xingqi, Hu Xing, Wang Yong, Min Longrui and Liu Zhujie, 2010. Paleoenvironmental and Paleoclimatic Changes During 47~25 ka BP as Indicated by Jing'erwa Section in Nihewan Basin. *Acta Geologica Sinica*, 84(7): 939–946 (in Chinese with English abstract).

Condie, K.C., 1993. Chemical composition and evolution of the upper continental crust: contrasting results from surface samples and shales. *Chemical geology*, 104(1): 1–37.

Cullers, R.L., 1994. The controls on the major and trace element variation of shales, siltstones, and sandstones of Pennsylvanian-Permian age from uplifted continental blocks in Colorado to platform sediment in Kansas, USA. *Geochimica et Cosmochimica Acta*, 58(22): 4955–4972.

Deng, C., Zhu, R., Zhang, R., Ao, H., and Pan, Y., 2008. Timing of the Nihewan formation and faunas. *Quaternary Research*, 69(1): 77–90.

Deng Qidong and You Huichuan, 1985. The structural activity and formation mechanism of the down-faulted basins around Ordos block. In: Institute of Geology, State Seismological Bureau (ed.), *Research on Recent Crustal Movement 1*, Beijing: Seismological Press, 58–78 (in Chinese).

Du Hengjian, Cai Baoquan, Ma Ancheng, Cheng Jie and Wu Weimin, 1988a. Late Cenozoic Biostratigraphic Zonation of the Nihewan Basin. *Earth Science-Journal of China University of Geosciences*, 20(1): 35–42 (in Chinese with English abstract).

Du Hengjian, Wang Ande, Zhao Qiqiang and Cai Baoquan, 1988b. A New Late Pliocene Stratigraphic Unit in the Nihewan Region: The Daodi Fm. *Earth Science-Journal of the China University of Geosciences*, 13(5): 561–568 (in Chinese with English abstract).

Floyd, P.A., Shail, R., Leveridge, B.E., and Franke, W., 1991. Geochemistry and provenance of Rhenohercynian synorogenic sandstones: implications for tectonic environment discrimination. *Geological Society, London, Special Publications*, 57(1): 173–188.

Floyd, P.A., Winchester, J.A., and Park, R.G., 1989. Geochemistry and tectonic setting of Lewisian clastic metasediments from the Early Proterozoic Loch Maree Group of Gairloch, NW Scotland. *Precambrian Research*, 45(1): 203–214.

Floyd, P.A., and Leveridge, B.E., 1987. Tectonic environment of the Devonian Gramscatho basin, south Cornwall: framework mode and geochemical evidence from turbiditic sandstones. *Journal of the Geological Society*, 144(4): 531–542.

Gill, J.B., 1981. Geophysical Setting of Volcanism at Convergent Plate Boundaries, In: *Orogenic Andesites and Plate Tectonics*. Berlin: Springer-Verlag, 44–63.

Girty, G.H., Ridge, D.L., Knaack, C., Johnson, D., and Al-Riyami, R.K., 1996. Provenance and depositional setting of Paleozoic chert and argillite, Sierra Nevada, California. *Journal of Sedimentary Research*, 66(1): 107–118.

Han Zhiyong, Li Xusheng, Wang Yong, Wang Xianyan, Yi Shuangwen and Lu Huayu, 2016. Tectonically-controlled infilling of the eastern Nihewan Basin, North China, since the middle Pleistocene. *Science China Earth Sciences*, 59(7): 1378–1389.

Hayashi, K., Fujisawa, H., Holland, H.D., and Ohmoto, H., 1997. Geochemistry of 1.9 Ga sedimentary rocks from northeastern Labrador, Canada. *Geochimica et Cosmochimica Acta*, 61 (19): 4115–4137.

Herron, M.M., 1988. Geochemical classification of terrigenous sands and shales from core or log data. *Journal of Sedimentary Research*, 58(5): 820–829.

Huang Wanbo and Tang Yingjun, 1974. Observations on the Late Cenozoic sections of the Nihewan basin. *Vertebrata Palasiatica*, 12(2): 99–108 (in Chinese with English abstract).

Li Deyong, Jiang Xiaodian, Xu Fa, Liu Jinshui and Hou Guowei, 2016. Geochemistry of the Paleocene Clastic Rocks in Lishui Sag, East China Sea Shelf Basin: Implications for Tectonic Background and Provenance. *Acta Geologica Sinica (English Edition)*, 90(1): 166–181.

Li Huamei, and Wang Junda, 1982. Magnetostratigraphic study of several typical geologic sections in North China. In: Liu Tungsheng (ed.), *Quaternary Geology and Environment of China*. Beijing: China Ocean Press, 33–37 (in Chinese with English abstract).

Li Qiugen, Chen Xu, Liu Shuwen, Wang Zongqi, Zhou Yingkui, Zhang Jian and Wang Tao, 2009. Evaluating the provenance of metasedimentary rocks of the Jiangxian Group from the Zhongtiao Mountain using whole-rock geochemistry and detrital zircon Hf isotope. *Acta Geologica Sinica (English Edition)*, 83(3): 550–561.

Li, W., Dong, Y., Guo, A., Liu, X., Wang, Y., Liu, W., and Yang, Y., 2015. Geochronology, geochemistry and Sr-Nd-Hf isotopes of mafic dikes in the Huicheng Basin: Constraints on intracontinental extension of the Qinling orogen. *Journal of Asian Earth Sciences*, 104: 115–126.

López, J.M.G., Bauluz, B., Fernández-Nieto, C., and Oliete, A.Y., 2005. Factors controlling the trace-element distribution in fine-grained rocks: the Albian kaolinite-rich deposits of the Oliete Basin (NE Spain). *Chemical geology*, 214(1): 1–19.

Mclennan, S.M., 1989. Rare earth elements in sedimentary rocks; influence of provenance and sedimentary processes. *Reviews in Mineralogy and Geochemistry*, 21(1): 169–200.

Mclennan, S.M., and Taylor, S.R., 1991. Sedimentary rocks and crustal evolution: tectonic setting and secular trends. *The Journal of Geology*, 99(1): 1–21.

Min Longrui, Chi Zhenqing, Wang Yong, Dong Jin, Wang Yulong and Zhu Guanxiang, 2015. Lithostratigraphic division and correlation of Haojiatai NHA borehole from Nihewan Basin in Yangyuan, Hebei. *Geology in China*, 42(4): 1068–1078 (in Chinese with English abstract).

Min Longrui, Zhang Zonghu, Wang Xisheng, Zheng Shaohua and Zhu Guanxiang, 2006. The basal boundary of the Nihewan formation at the Taiergou section of Yangyuan, Hebei Province. *Journal of Stratigraphy*, 30(2): 103–108 (in Chinese with English abstract).

Peltzer, G., Tapponnier, P., Zhang, Z., and Xu, Z.Q., 1985. Neogene and Quaternary faulting in and along the Qinling Shan. *Nature*, 317(6037): 500–505.

Pettijohn, F.J., Potter, P.E., and Siever, R., 1987. *Sand and sandstone, Second Edition*. Berlin: Springer-Verlag, 553.

Shi, W., Dong, S., Liu, Y., Hu, J., Chen, X., and Chen, P., 2015a. Cenozoic tectonic evolution of the South Ningxia region, northeastern Tibetan Plateau inferred from new structural investigations and fault kinematic analyses. *Tectonophysics*, 649: 139–164.

Shi, W., Cen, M., Chen, L., Wang, Y., Chen, X., Li, J., and Chen, P., 2015b. Evolution of the late Cenozoic tectonic stress regime in the Shanxi Rift, central North China Plate inferred from new fault kinematic analysis. *Journal of Asian Earth Sciences*, 114: 54–72.

Singer, B.S., Hoffman, K.A., Chauvin, A., Coe, R.S., and Pringle, M.S., 1999. Dating transitionally magnetized lavas of the late Matuyama Chron: Toward a new 40Ar/39Ar timescale of reversals and events. *Journal of Geophysical Research: Solid Earth*, 104(B1): 679–693.

Singh, P., and Rajamani, V., 2001. REE geochemistry of recent clastic sediments from the Kaveri floodplains, southern India: implication to source area weathering and sedimentary processes. *Geochimica et Cosmochimica Acta*, 65(18): 3093–3108.

Su Pu, Reidar Lovlie, Fan Xingzhao and Zhao Zengjian, 2000. A high-resoulution magnetostratigraphy study on the Nihewan Group at Xujiayao. *Chinese Journal of Geophysics*, 43(2): 223–231.

Sun, J., 2005. Long-term fluvial archives in the Fen Wei Graben, central China, and their bearing on the tectonic history of the India? Asia collision system during the Quaternary. *Quaternary Science Reviews*, 24(10–11): 1279–1286.

Sun Jiaopeng, Chen Shiyue, Ma Yinsheng, Peng Yuan, Shao Pengcheng, Ma Shuai, Dai Kun and Zheng Ce, 2016. Early Ordovician Continental Arc Collision and Retroarc Foreland Basin on the Northern Margin of Qaidam Basin: Geochemical Evidence from Clastic Rocks. *Acta Geologica Sinica*, 90(1): 80–92 (in Chinese with English abstract).

Sun Zhenjun, Sun Guosheng, Yu Henan, Tian Yi, Liu Shanli, Xiang Zhu, Meng Jian, Xue Huaiyu and Lu Lina, 2015. Geochronology and geochemical characteristics of intrusion in the Jinchangliang Gold deposit, Inner Mongolia and their tectonic significance. *Acta Geologica Sinica* (English Edition), 89(6): 1947–1962.

Tapponnier, P., Peltzer, G., and Armijo, R., 1986. On the mechanics of the collision between India and Asia. *Geological Society, London, Special Publications*, 19(1): 113–157.

Taylor, S.R., and Mclennan, S.M., 1985. *The continental crust: its composition and evolution*. Oxford: Blackwell Scientific Publications, 312.

Wang Ande, 1982. Discovery of the Pliocene Mammalian faunas from the Nihewan region and its significance. *Chinese Science Bulletin*, 27(4): 227–229 (in Chinese with English abstract).

Wang Chengshan and Li Xianghui, 2003. *Sedimentary basin: from principles to analyses*. Beijing: China Higher Education Press, 378 (in Chinese).

Wang Hongqiang, Deng Chenglong, Zhu Rixiang and Xie Fei, 2006. Paleomagnetic dating of the Cenjiawan Paleolithic site in the Nihewan Basin, northern China. *Science in China* (Series D), 49(3): 295–303 (in Chinese with English abstract).

Wang Nailiang, Yang Jingchun, Xia Zhengkai, Mo Duowen, Li Youli and Pan Mao, 1996. *The sediment in Cenozoic and structural landform in Shanxi Graben*. Beijing: Science Press, 409 (in Chinese).

Wang, W., Kirby, E., Zhang, P., Zhen, D., Zhang, G., Zhang, H., Zhen, W., and Chai, C., 2013. Tertiary basin evolution along the northeastern margin of the Tibetan Plateau: Evidence for basin formation during Oligocene transtension. *Geological Society of America Bulletin*, 125(3–4): 377–400.

Wang Yunsheng, 1989. Sedimentary facies and succession of Nihewan Formation in Yangyuan County of Hebei Province. *Marine Geology & Quaternary Geology*, 9(1): 85–92 (in Chinese with English abstract).

Xu, X., Ma, X., and Deng, Q., 1993. Neotectonic activity along the Shanxi rift system, China. *Tectonophysics*, 219(4): 305–325.

Xu Yong, Yue Leping, Li Jianxing, Sun Lu, Sun Bo, Zhang Jiayin, Ma Ji and Wang Jianqi, 2012. Red clay deposits on the Chinese Loess Plateau during 11.0–2.6 Ma and its implications for long-term evolution of East Asian monsoon. *Environmental Earth Sciences*, 66(7): 2021–2030 (in Chinese with English abstract).

Yan Quanren, Gao Shanling, Wang Zongqi, Li Jiliang, Xiao Wenjiao, Hou Quanling, Yan Zhen and Chen Haihong, 2002. Geochemical constraints of sediments on the provenance, depositional environment and tectonic setting of the songliao prototype basin. *Acta Geologica Sinica* (English Edition), 76 (4): 455–462.

Yang Zongyao, Tang Juxing, Lang Xinghai, Zhang Zhong, Zhang Jinshu, Gao Yiming, Huang Yong, Xie Fuwei, Yangang Fu and Wang Yong, 2017. Geochemical Characteristics of the Jurassic Sandstones in the Xiongcun Copper-Gold Deposit,Tibet:Constraints on Tectonic Setting. *Acta Geologica Sinica*, 91(9): 1985–2003 (in Chinese with English abstract).

Yin, A., 2010. Cenozoic tectonic evolution of Asia: A

preliminary synthesis. Tectonophysics 488(1–4): 293–325.

Yu Xin, Yang Jianghai, Liu Jianzhong, Du Yuansheng and Chai Rong, 2017. Provenance of the Late Permian Longtan Formation in SW Guizhou Province and Implication for Reconstruction of Regional Sedimentation and Paleogeography. *Acta Geologica Sinica*, 91(6): 1374–1385 (in Chinese with English abstract).

Zhang Peizhen, Deng Qidong, Zhang Guomin, Ma Jin, Gan Weijun, Min Wei, Mao Fengying and Wang Qi., 2003. Active tectonic blocks and strong earthquakes in the continent of China. *Science in China* (Series D), 46(2): 13–24 (in Chinese with English abstract).

Zhang, Y.Q., Mercier, J.L., and Vergély, P., 1998. Extension in the graben systems around the Ordos (China), and its contribution to the extrusion tectonics of south China with respect to Gobi-Mongolia. *Tectonophysics*, 285(1–2): 41–75.

Zhang, Y., Ma, Y., Yang, N., Shi, W., and Dong, S., 2003. Cenozoic extensional stress evolution in North China. *Journal of Geodynamics*, 36(5): 591–613.

Zhang Yueqiao, Vergely Pierre, Mercier Jacques-Louis, Wang Yongmin, Zhang Yong and Huang Dezhi., 1999. Kinematic History and Changes in the Tectonic Stress Regime during the Cenozoic along the Qinling and Southern Tanlu Fault Zones. *Acta Geologica Sinica* (English Edition), 73(3): 264–274.

Zhao Xiaochen, Liu Chiyang, Wang Jianqiang, Duan Liang, Zhao Yan, Zhang Qihang and Luo Wei, 2017. Petrology, Geochemistry and Zircon U-Pb Geochronology of the Xiangshan Group in the Eastern Hexi Corridor Belt: Implications for Provenance and Tectonic Evolution. *Acta Geologica Sinica* (English Edition), 91(5): 1680–1703.

Zhu, R.X., Potts, R., Xie, F., Hoffman, K.A., Deng, C.L., Shi, C.D., Pan, Y.X., Wang, H.Q., Shi, R.P., Wang, Y.C., Shi, G.H., and Wu, N.Q., 2004. New evidence on the earliest human presence at high northern latitudes in northeast Asia. *Nature*, 431(7008): 559–562.

About the first author

LIU Jin, female, born in 1987 in Yuncheng City, Shanxi Province, China. She is now working in School of Civil and Architecture Engineering, Xi'an Technological University. She is interested in Quaternary geology, structural geology and Global Change. E-mail: liujin_1203@163.com. Address: No.2 Xuefu Middle Road, Weiyang District, Xi'an, Shaanxi Province 710021, China.